Loss-of-Function Mutation in PTPN2 Causes Aberrant Activation of JAK Signaling Via STAT and Very Early Onset Intestinal Inflammation

Marianna Parlato, Qing Nian, Fabienne Charbit-Henrion, Frank Ruemmele, Fernando Rodrigues-Lima, Nadine N. Cerf-Bensussan

Gastroenterology 2020;159:1968–1971

BRIEF COMMUNICATIONS

Loss-of-Function Mutation in PTPN2 Causes Aberrant Activation of JAK Signaling Via STAT and Very Early Onset Intestinal Inflammation

Marianna Parlato,[1,*] **Qing Nian**,[2,3,*] Fabienne Charbit-Henrion,[1,4] Frank M. Ruemmele,[1,4] Fernando Rodrigues-Lima,[2,§] and Nadine Cerf-Bensussan,[1,§] and members of the Immunobiota Study Group

[1]*Université de Paris, Imagine Institute, Laboratory of Intestinal Immunity, Inserm, UMR1163, F-75015, Paris, France;* [2]*Université de Paris, Unité de Biologie Fonctionnelle et Adaptative, CNRS UMR 8251, Paris, France;* [3]*Hospital of Chengdu University of Traditional Chinese Medicine, Chengdu, China; and* [4]*Department of Pediatric Gastroenterology, Assistance Publique-Hôpitaux de Paris, Hôpital Necker-Enfants Malades, F-75015, Paris, France.*

Keywords: Autoimmunity; Immune Regulation; PTPN2; VEO-IBD.

Genome-wide association studies have linked non-coding single-nucleotide polymorphisms in the *PTPN2* locus to several immuno-mediated diseases, including inflammatory bowel diseases, celiac disease, type 1 diabetes, and rheumatoid arthritis.[1] *PTPN2* encodes an ubiquitous non-receptor protein tyrosine phosphatase that exerts a negative feedback on the JAK-STAT pathway.[2] A key immunoregulatory role of PTPN2 is suggested by studies in mice. Thus, *ptpn2−/−* mice developed severe lethal systemic inflammation and diarrhea,[1] whereas T-cell–specific loss of *ptpn2* led to peripheral T-cell expansion and autoimmunity and increased susceptibility to intestinal inflammation.[1] Loss of one p*tpn2* copy was sufficient to promote inflammation in a T-cell–mediated model of arthritis,[3] overall stressing the importance of 2 functional copies of PTPN2 to prevent excessive T-cell activation. Yet, the exact role of PTPN2 in humans remains to be determined. Herein, we identify *PTPN2* haploinsufficiency as a novel monogenic cause of autoimmune enteropathy and illustrate how monogenic diseases provide the opportunity to validate genes or pathways identified by genome-wide association studies, bridging the gap between polyfactorial forms of intestinal inflammation and single-gene defects.

Methods

Available in the Supplementary Methods.

Results

Within our cohort of patients with very early onset inflammatory bowel disease,[4] a 3-year-old girl (P1) born from healthy non-consanguineous parents presented with severe chronic secretory diarrhea and eczema since the age of 3 months. Immunological work-up was normal except for high titers of serum anti-AIE75 antibody. Duodenal biopsies showed severe villous atrophy with massive lymphocyte infiltration. Diarrhea improved on parenteral nutrition and treatment with steroids, azathioprine, and tacrolimus, but clinical and histological remission was observed only after switching to sirolimus (Figure 1*A*). Targeted sequencing excluded a molecular defect in *FOXP3, CTLA4, LRBA, STAT3,* and *CD25*, known causes of autoimmune enteropathy.[4] Whole exome sequencing was performed on parents-proband-trio's DNA and identified a de novo and rare heterozygous missense variant in exon 6 of the *PTPN2* gene (NM_002828.3 c.646T>G, chr18:12,785,478-12,929,643) replacing a cysteine residue with a glycine in position 216 (Supplementary Table 1). Sanger sequencing confirmed familial segregation (Figure 1*B–D*). Overexpression of C216G-PTPN2 and of the wild-type (WT) allele in HEK293T cells yielded comparable amount of protein (Figure 1*E*). Expression of endogenous PTPN2 protein was also comparable in patient and control-derived Epstein-Barr virus–transformed B-cell lines (B-EBV) (Figure 1*F*), indicating that the c.646T>G mutation does not impact PTPN2 expression. The variant was indicated to be damaging by all prediction tools (Combined Annotation Dependent Depletion score: 25.2) (Supplementary Table 1). Cys216 is strongly conserved across species and part of the "PTP signature motif" (HC[X5]R) (Figure 1*G*), which forms the phosphate-binding loop in the core of the catalytic site in all members of the PTP family.[5] Cys216 initiates catalysis, via its thiolate group, by mounting nucleophilic attack of phosphate substrates (Figure 1*H*). Replacement of cysteine with glycine should impair catalysis, as glycine lacks the polar side chain to interact with phosphotyrosyl residues. WT and mutant C-terminally tagged PTPN2 were transiently expressed in HEK293T cells, immunoprecipitated, and de-phosphorylation of STAT1 peptides, which are putative substrates of PTPN2,[2] was measured. Compared with WT-PTPN2, the mutant enzyme was, as anticipated, totally deprived of catalytic activity (Figure 1*I*). Lentiviral constructs encoding WT- or C216G-PTPN2 were next used to

*Authors share co-first authorship; §Authors share co-senior authorship.

Abbreviations used in this paper: EBV, Epstein-Barr virus; GOF, gain of function; IL, interleukin; TCR, T-cell receptor; TRE, transcriptional response element; WT, wild type.

Most current article

0016-5085
https://doi.org/10.1053/j.gastro.2020.07.040

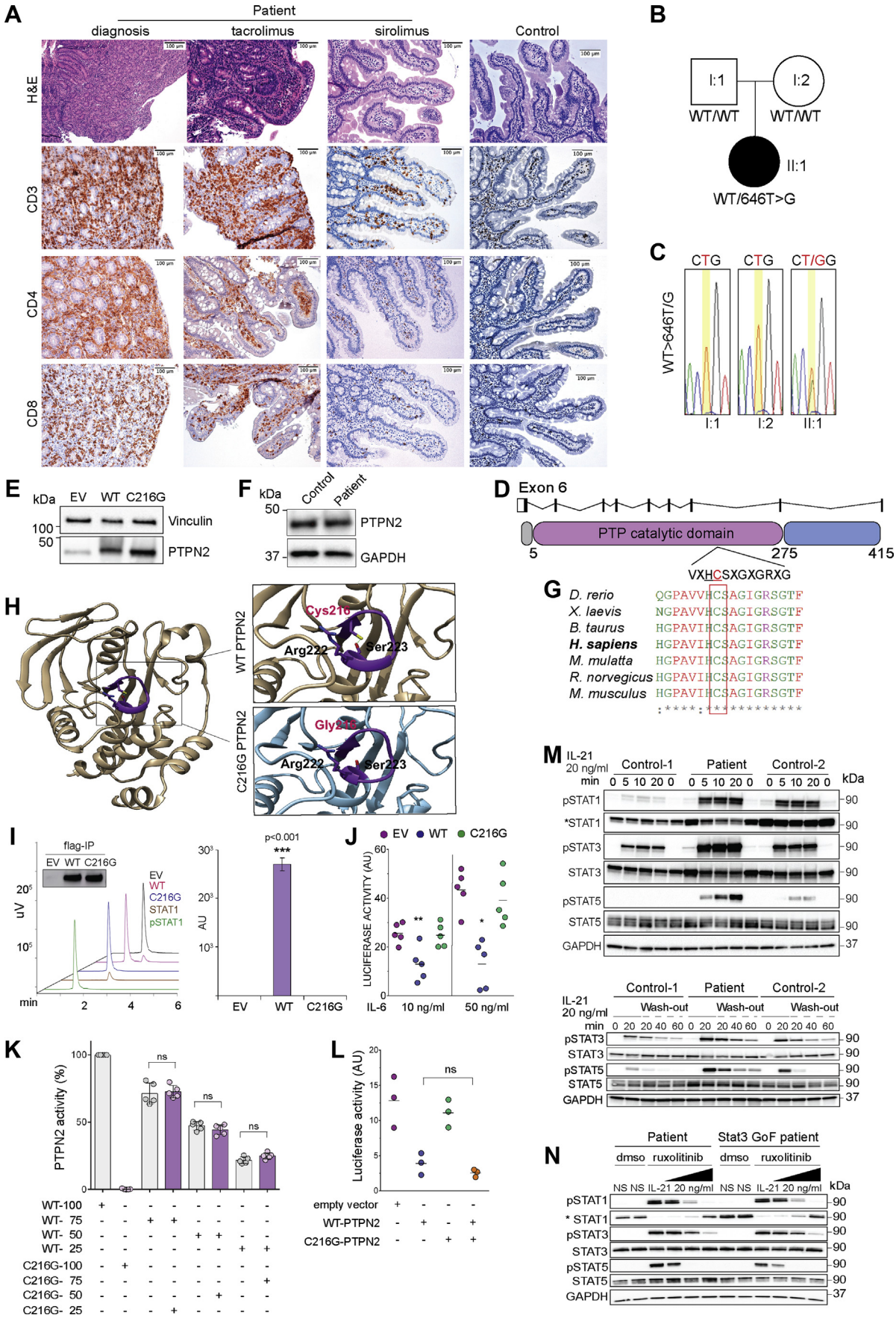
A
Patient
diagnosis
tacrolimus
sirolimus
Control
H&E
CD3
CD4
CD8
B
I:1
I:2
WT/WT
WT/WT
II:1
WT/646T>G
C
CTG
CTG
CT/GG
WT>646T/G
I:1
I:2
II:1
D
Exon 6
PTP catalytic domain
5
275
415
VXHCSXGXGRXG
E
kDa
EV
WT
C216G
100
50
Vinculin
PTPN2
F
kDa
Control
Patient
50
37
PTPN2
GAPDH
G
D. rerio QGPAVVHCSAGIGRSGTF
X. laevis NGPAVVHCSAGIGRSGTF
B. taurus HGPAVIHCSAGIGRSGTF
H. sapiens HGPAVIHCSAGIGRSGTF
M. mulatta HGPAVIHCSAGIGRSGTF
R. norvegicus HGPAVIHCSAGIGRSGTF
M. musculus HGPAVIHCSAGIGRSGTF
H
WT PTPN2
C216G PTPN2
Cys216
Arg222
Ser223
Gly216
I
flag-IP
EV WT C216G
EV
WT
C216G
STAT1
pSTAT1
uV
min
2
4
6
p<0.001
***
AU
EV
WT
C216G
J
EV
WT
C216G
LUCIFERASE ACTIVITY (AU)
**
*
IL-6
10 ng/ml
50 ng/ml
M
IL-21
20 ng/ml
min
Control-1
Patient
Control-2
0 5 10 20 0
kDa
pSTAT1
*STAT1
pSTAT3
STAT3
pSTAT5
STAT5
GAPDH
90
37
Wash-out
0 20 20 40 60
K
PTPN2 activity (%)
ns
WT-100
WT- 75
WT- 50
WT- 25
C216G-100
C216G- 75
C216G- 50
C216G- 25
L
Luciferase activity (AU)
ns
empty vector
WT-PTPN2
C216G-PTPN2
N
Patient
Stat3 GoF patient
dmso
ruxolitinib
NS NS IL-21 20 ng/ml
kDa
pSTAT1
* STAT1
pSTAT3
STAT3
pSTAT5
STAT5
GAPDH

transduce HEK293T cells stably expressing a luciferase reporter gene under the control of STAT3 transcriptional response elements (TRE). Following interleukin (IL)-6 stimulation, overexpression of WT-PTPN2 led to significant downregulation of STAT3-TRE activity over control, whereas the mutant form of PTPN2 failed to do so (Figure 1*J*). Mixes of recombinant WT and C216G-PTPN2 displayed in vitro phosphatase activity proportional to the amount of WT PTPN2 (Figure 1*K*) and co-transfection of C216G-PTPN2 and WT-PTPN2 repressed STAT3 transcriptional activity in IL-6–stimulated HEK293T-STAT3-TRE cells similarly as transfection by WT-PTPN2 alone (Figure 1*L*), overall indicating that C216G-PTPN2 does not exert a dominant negative effect. We next compared the impact of PTPN2 deficiency on either T-cell receptor (TCR) activation or JAK-STAT signaling. Although TCR ligation with anti-CD3 antibody induced comparable Ca^{2+} mobilization, same global pattern of tyrosine phosphorylation and comparable ERK1/2 and LCK phosphorylation in control and patient T-cell blasts, phosphorylation of STAT3 in response to IL-15 was increased in patient T-cell blasts (Supplementary Figure 1*A*–*C*). Similarly, WT and PTPN2-depleted Jurkat cells displayed comparable ERK1/2 and LCK phosphorylation after TCR activation but increased phosphorylation of STAT1 in response to interferon-gamma (Supplementary Figure 1*D* and *E*). Hyperactivation of JAK-STAT pathway was confirmed in the patient's EBV-B cells. IL-21–induced phosphorylation of STAT3 was increased and prolonged in the patient's EBV-B cells compared with 2 controls (Figure 1*M*). Furthermore, phosphorylation of STAT5 and STAT1, which were not triggered by IL-21 in control EBV-B cells, was observed in the patient's cells, pointing to alternative reprogramming of JAK-STAT signaling. Prominent STAT3 phosphorylation was also detected in intestinal lamina propria at time of disease activity (Supplementary Figure 1*F*). Importantly, Food and Drug Administration–approved JAK inhibitor, ruxolitinib, inhibited STAT phosphorylation in patient-derived B-EBV cells as efficiently as in cells derived from STAT3 gain-of-function (GOF) patient (Figure 1*N*).

Discussion

Here, we identify PTPN2 haploinsufficiency as a monogenic cause of intestinal autoimmunity. In line with the lack of therapeutic efficacy of tacrolimus, a calcineurin inhibitor that blocks Ca^{2+}-dependent signaling downstream of TCR, the defect did not affect TCR signaling. In contrast, impaired negative regulation of JAK-STAT signaling was observed in the patient's lymphocytes. Severe autoimmune enteropathy or enterocolitis is also a hallmark of STAT3 GOF mutations,[6,7] overall highlighting the crucial need of tightly regulating JAK-STAT activation to restrict intestinal inflammation. The very recent identification of monoallelic loss-of-function *PTPN2* mutation in a young man presenting with common variable immunodeficiency and arthritis and in his mother presenting with lupus, type I diabetes, thyroiditis, and cytopenia[8] supports the disease-causing role of PTPN2 haploinsufficiency and illustrates the known pleiotropy of mutations enhancing JAK-STAT signaling.[6] We have previously shown that durable remission can be achieved by ruxolitinib in severe enterocolitis associated with *STAT3* GOF mutation.[7] Herein, the pharmacological rescue of JAK-STAT hyperactivation in patient's cells by ruxolitinib

Figure 1. PTPN2 mutation in a patient with early-onset intestinal autoimmunity. (*A*) Hematoxylin and eosin (H&E) and CD3, CD4, CD8 staining of duodenal biopsies in the patient with autoimmune enteropathy at diagnosis at 6 months, under tacrolimus treatment at 12 months, and under sirolimus treatment at 27 months and in the 4-year-old control with normal intestinal histology. (*B*) Pedigree showing de novo heterozygous mutation in *PTPN2*. (*C*) Sanger-sequencing electropherograms for the affected individual and parents. (*D*) Exon structure of the *PTPN2* gene and domain structure of the PTPN2 protein. (*E*) WT and C216G-PTPN2 protein expression in transduced HEK293T cells carrying STAT3-responsive elements (STAT-TRE). (*F*) Endogenous PTPN2 protein expression in patient- and control-derived EBV cells. (*G*) Multiple alignments of PTPN2 orthologs from different species using the Clustal Omega software. The affected amino acid is boxed in red. Conserved residues are indicated as follows: full identity (*), similar characteristics (:) (>0.5 in the Gonnet PAM 250 matrix), weak similarities (.) (<0.5 in the Gonnet PAM 250 matrix). (*H*) Mapping of Cys216 onto the crystal structure of human PTPN2 (Protein Data Bank [PDB] accession 1L8K). The catalytic cysteine residue of PTPN2 (Cys216) and 2 other important residues also present in the PTP-Loop (Arg222 and Ser223) are shown in sticks. The zoomed-in region (with the structure rotated 90° toward the reader) shows the position of Cys216 (red), Arg222, and Ser223. The hydrogen bond between the lateral chains of Cys216 and Ser223 is shown with green dots. (*I*) Tyrosine phosphatase activity of immunoprecipitated WT and C216G-PTPN2 toward fluorescent tyrosine-phosphorylated Stat1 peptide by RP-UFLC. RP-UFLC chromatograms are shown for control peptides (FAM-pStat1 and FAM-Stat1) and for immunoprecipitates from empty vector, WT, and C216G PTPN2 transfected HEK cells. PTPN2 activity toward pStat1 is shown in arbitrary units. Results are representative of 3 experiments in triplicate. (*J*) STAT3 transcriptional activity following 48-hour activation with IL-6 (10 ng/mL) of HEK293T cells expressing STAT3-responsive elements (TRE) and stably transduced with empty vector (EV), WT-PTPN2, and C216G-PTPN2. The mean of 5 independent experiments is indicated). (*K*) PTPN2 activity of 50 nM (final concentration) of purified WT- and C216G-PTPN2 at different ratios (100% WT/0% C216G; 75% WT/25% C216G; 50% WT/50% C216G; 25% WT/75% C216G; 0% WT/100% C216G). Results represent the mean of 5 independent experiments. (*L*) STAT3 transcriptional activity following 48-hour activation with IL-6 (10 ng/mL) of HEK293T cells expressing STAT3-responsive elements (TRE) and transfected with empty vector (EV), WT-PTPN2 and C216G-PTPN2 or both a 1:1 vector ratio. The mean of 3 independent experiments is shown. (*M*) Immunoblot of EBV-LCLs from 2 healthy controls and patient after activation with IL-21 (20 ng/mL) for indicated time points (top) or after wash-out of IL-21 (bottom). Data representative of 2 independent experiments. (*N*) In vitro assessment of 2, 20, and 200 μM ruxolitinib efficacy following IL-21 (20 ng/mL) stimulation of EBV-B cells derived from the C216G-PTPN2 patient and from a patient with constitutive T716M-STAT3 GOF mutation. NS, not stimulated. *STAT1 antibody preferentially recognizes the nonphosphorylated form of STAT1 (ns, nonsignificant, $^{*}P < .05$, $^{**}P < .01$, $^{***}P < .001$, 1-way analysis of variance).

suggests that JAK inhibitors may be used to treat PTPN2 deficiency and more generally inflammatory disorders associated with excessive JAK-STAT signaling.

Supplementary Material

Note: To access the supplementary material accompanying this article, visit the online version of *Gastroenterology* at www.gastrojournal.org, and at https://doi.org/10.1053/j.gastro.2020.07.040.

References

1. Pike KA, Tremblay ML. Front Immunol 2018;9:2504.
2. Simoncic PD, et al. Curr Biol 2002;12:446–453.
3. Svensson MND, et al. J Clin Invest 2019;129:1193–1210.
4. Charbit-Henrion F, et al. J Crohn's Colitis 2018;12:1104–1112.
5. Tonks NK. Nat Rev Mol Cell Biol 2006;7:833–846.
6. Fabre A, et al. J Allergy Clin Immunol Pract 2019;7:1958–1969.
7. **Parlato M, Charbit-Henrion F**, et al. Gastroenterology 2019;156:1206–1210.
8. Thaventhiran JED, et al. Nature 2020;583:90–95.

Author names in bold designate shared co-first authorship.

Received April 20, 2020. Accepted July 21, 2020.

Correspondence
Address correspondence to: Nadine Cerf-Bensussan, MD, PhD, Université de Paris, Imagine Institute, Laboratory of Intestinal Immunity, Inserm, UMR1163, F-75015, Paris, France. e-mail: nadine.cerf-bensussan@inserm.fr.

Acknowledgments
Members of the Immunobiota Study Group are as follows: Bernadette Bègue (Université de Paris, Imagine Institute, Laboratory of Intestinal Immunity, Inserm, UMR1163, Paris, France), Jeremy Berthelet (Université de Paris, Unité de Biologie Fonctionnelle et Adaptative, CNRS UMR 8251, Paris, France), Kaan Boztug (St. Anna Children's Cancer Research Institute (CCRI), Ludwig Boltzmann Institute for Rare and Undiagnosed Diseases, CeMM Research Center for Molecular Medicine, Austrian Academy of Sciences, Department of Pediatrics and Adolescent Medicine, Medical University of Vienna, St. Anna Children's Hospital, Department of Pediatrics and Adolescent Medicine, Medical University of Vienna, Vienna, Austria), Rémi Duclaux-Loras (Université de Paris, Imagine Institute, Laboratory of Intestinal Immunity, Inserm, UMR1163, Assistance Publique-Hôpitaux de Paris, Hôpital Necker-Enfants Malades, Service de Gastroentérologie pédiatrique, Paris, France), Sylvain Latour (Université de Paris, Imagine Institute, Laboratory of Lymphocyte Activation and Susceptibility to EBV infection, Inserm, UMR1163, Paris, France), Marco Maggioni (Fondazione IRCCS Ca' Granda-Ospedale Maggiore Policlinico, University of Milan, Milan, Italy), Emmanuel Martin (Université de Paris, Imagine Institute, Laboratory of Lymphocyte Activation and Susceptibility to EBV infection, Inserm, UMR1163, Paris, France), Thierry-Jo Molina (Pathology Department, Necker-Enfants Malades University Hospital, AP-HP, Paris, France), Julia Pazmandi (St. Anna Children's Cancer Research Institute, Ludwig Boltzmann Institute for Rare and Undiagnosed Diseases, CeMM Research Center for Molecular Medicine, Austrian Academy of Sciences, Vienna, Austria), and Frederic Rieux-Laucat ((Université de Paris, Imagine Institute, Laboratory of Immunogenetics of Paediatric Autoimmunity, Inserm, UMR1163, Paris, France).

We thank the patients and their families. We thank the technical platform "Bioprofiler UFLC" from the BFA Unit for provision of UFLC facilities, Prof Emanuele Bosi for anti-AIE75 serum measurement, and Dr Jules Gilet for his careful and critical reading of our paper.

CRediT Authorship Contributions
Marianna Parlato, PhD (Conceptualization: Lead; Data curation: Lead; Formal analysis: Lead; Methodology: Lead; Supervision: Supporting; Writing – original draft: Lead; Writing – review & editing: Lead). Qing Nian, PhD (Data curation: Equal; Methodology: equal; Formal analysis: Equal). Fabienne Charbit-Henrion, MD, PhD (patient care coordination and clinical samples acquisition.: Lead). Frank Ruemmele, MD, PhD (patient care coordination and clinical samples acquisition.: Supporting). Fernando Rodrigues-Lima, PhD (Supervision: Equal; Writing – original draft: Equal). Nadine Cerf-Bensussan, MD, PhD (Conceptualization: Equal; Supervision: Lead; Writing – original draft: Equal; Writing – review & editing: Lead).

Conflict of interest
The authors disclose no conflicts.

Funding
The work was supported by institutional grants from INSERM, by the European grant ERC-2013-AdG-339407-IMMUNOBIOTA, by the Investissement d'Avenir grant ANR-10-IAHU-01, by the Fondation Princesse Grace, by Fondation Maladies Rares to Nadine Cerf-Bensussan and by institutional grants from Paris Diderot University and CNRS to Fernando Rodrigues-Lima. Qing Nian was supported by a PhD fellowship from the China Scholarship Council.

Supplementary Methods

Clinical Study

The patient was included within the Immunobiota protocol.[1] Recruitment of patients was based on severe chronic diarrhea developed before 6 years of age and refractory to medical treatment as previously described.[1] Informed consent for functional and genetic studies was obtained from a parent or a legal guardian in accordance with the Declaration of Helsinki under institutional review board–approved protocol (CPP Ile-de-France II).

Histology and Immunohistochemistry

Patient duodenal biopsies were obtained at 6, 12, and at 27 months. Control duodenal biopsies were obtained from a 4-year-old boy who underwent endoscopy for unconfirmed suspicion of eosinophilic gastroenteritis and from a previously described patient with STAT3 GOF mutation.[2] Biopsies were fixed in 4% buffered formalin for 24 hours, paraffin-embedded, and stained with hematoxylin & eosin. CD3 (polyclonal; Dako, Glostrup, Denmark), CD4 (L26 clone; Dako), CD8 (C8/144B clone; Dako) immunophenotyping was performed on a Dako Omnis automated immunostainer. P-STAT3 (3E2; Cell Signaling, Danvers, MA) antibody was used according manufacturer's instructions.

DNA Sequencing

Whole-exome and targeted panel sequencing were performed as previously described.[1] For Sanger sequencing, primer sequences and polymerase chain reaction amplification conditions are available on request.

Variant Prioritization of Whole Exon Sequencing Data

Candidate variants were ranked by filtering out common polymorphisms with Minor Allele Frequency (MAF) $>1\%$. Potential causality of each protein-coding variant with MAF $<1\%$ was assessed using the Genome Aggregation Database (gnomAD) and the Institut Imagine database of 13,465 exomes from families affected with genetic diseases. OMIM, evolutionary conservation, and prediction tools (SIFT, PolyPhen2.2.2, Mutation Taster, combined annotation-dependent depletion [CADD]), together with mutation significance cutoff (MSC), a gene-level specific cutoff for CADD scores.[3,4]

Plasmid and Lentivirus Generation

The pCMV6 vector containing the full complementary DNA sequence of hPTPN2 (NM_080422) (Origene, Rockville, MD) was used to introduce the variant with the GENEART Site-Directed Mutagenesis System (Invitrogen, Carlsbad, CA). The mutation was confirmed by Sanger sequencing. WT and mutant constructs were subcloned into the pLVX-EF1α-IRES-mCherry Vector (Clontech, Mountain View, CA). Supernatant containing lentivirus particles was generated from Lenti-X^{TM}293T cells co-transfected with transfer plasmid, packaging pMD2.G (12259; Addgene, Cambridge, MA) and VSV-G envelope expressing psPAX2 (12260; Addgene) plasmids using Lipofectamine 2000 (Invitrogen). The virus-containing medium was 0.45-μm-filtered and used to transduce cells in the presence of polybrene (4 μg/mL). mCherry-positive cells were sorted by fluorescence-activated cell sorting (FACS) 5 days post-transduction.

PTPN2 Catalytic Activity Assays

Lenti-X^{TM}293T cells were transfected with FLAG-WT-PTPN2, FLAG-C216G-PTPN2 or empty vector (EV) (Origene). Twenty-four hours post-transfection, cells were washed with phospate-buffered saline (PBS) and resuspended in lysis buffer (PBS, 0.5% Triton X-100, protease inhibitors cocktail). The lysate was cleared by centrifugation (15,000*g* for 10 minutes at 4°C) and total protein concentration measured with Bradford reagent. For PTPN2 immunoprecipitation, 1 mg of whole-cell extracts (200 μL) were incubated overnight with 1 μg of an anti-flag mouse monoclonal antibody (Origene) at 4 °C. PTPN2 catalytic activity assay toward FAM-pStat1 peptide in immunoprecipitate was performed as previously described.[5] For testing dominant negative activity, untagged recombinant WT and C216G PTPN2 were produced in *Escherichia coli* as described[5,6] and mixed at different ratios to reach a total concentration of 50 nM in 100 mM sodium acetate, pH6 buffer containing 10 mM p-nitrophenyl phosphate. The dephosphorylated product was measured by absorbance at 405 nm at 37°C using a thermostated microplate reader (BioTek, Saint-Jean-de-Védas, France).

Protein Sequence Alignment

ClustalW2[7] was used to align protein sequences obtained from the National Center for Biotechnology Information with the following RefSeq accession numbers: NP_536347.1, NP_446442.1, NP_001120649.1, NP_997819.1, NP_001030508.1, AFH27310.1, NP_001086910.1.

Modeling of PTPN2-C216G Mutation

The C216G-PTPN2 mutation was created and analyzed using Swiss-PdbViewer[8] with human PTPN2 structure as template (PDB entry: 1L8K). Structures were rendered using Chimera.[9]

Cell Culture

Lenti-X^{TM}293T cells (Clontech) were cultured in Dulbecco's modified Eagle's Medium–Glutamax supplemented with 10% fetal calf serum (FCS) and penicillin-streptomycin (100 U/mL each; Invitrogen).

Expansion of T-cell blasts from peripheral blood mononuclear cells (PBMCs) was obtained by 3-day incubation with 1 μg/mL phytohemagglutinin (PHA) (Sigma-Aldrich, St Louis, MO) in RPMI 1640 Glutamax supplemented with 1% nonessential amino acids, 1% sodium pyruvate, 1% Hepes (Invitrogen), and 10% inactivated human serum AB (PAA). PHA-stimulated PBMCs were next cultured with 50U/mL IL-

2 (R&D Systems, Minneapolis, MN) for 2 to 3 weeks. Epstein-Barr–transformed B-cell lines were generated from frozen PBMCs of the patient, controls and from T716M STAT3 GOF patient, as previously described.[2] Jurkat cells were cultured in RPMI supplemented with 10% FCS, 20 mM Hepes, and penicillin-streptomycin.

Luciferase STAT3 Reporter Assay

Lenti-X^{TM}293T cells expressing STAT3 transcriptional responsive element (STAT3-TRE) were transduced with lentiviral particles expressing WT or PTPN2 C216G or EV. Each cell line was plated at 1×10^5 cells/well (24-well plate), stimulated with 5 ng/mL or 50 ng/mL IL-6 and, after 48 hours, luciferase was assayed with the Dual-Luciferase Reporter assay system (Promega, Madison, WI) following the manufacturer's instructions. All experiments were performed in duplicate.

For testing possible C216G dominant activity, STAT3-TRE-HEK293T cells were transfected with 50 ng of WT construct and/or mutant C216G (1:1) with Lipofectamine 2000 (ThermoFisher, Waltham, MA). Twenty-four hours post-transfection, the cells were treated with 5 ng/mL IL-6 for 48 hours and luciferase was assayed with the Dual-Luciferase Reporter assay system (Promega). All transfection experiments were performed in triplicate.

Antibodies

The following antibodies were used for immunoblotting with standard procedures: anti-PTPN2 (F8) from SantaCruz Biotechnology (Dallas, TX), anti-STAT1 (9H2), anti-pSTAT1 (58D6), anti-STAT3 (124H6), anti-pSTAT3 (3E2), anti-GAPDH-HRP (14C10), anti-ptyrosine (Tyr-100), anti-pERK1/2 (4376S), anti-ERK 1/2 (4695S), and anti-Ku70 (4103S), all from Cell Signaling; anti-pLCK Y505 (755216) and anti-pLCK Y394 (755103) from Novus Biologicals (Littleton, CO).

CRISPR-Cas9 Genome Editing

Single-guide RNAs (sgRNAs) were designed using the CRISPR Design Tool (Massachusetts Institute of Technology) and cloned into the BsmbI site of LentiCRISPRv2 plasmid (8290; Addgene). sgRNA sequences are available on request. Following production of lentiviral particles, the lenti-CRISPRv2 plasmids were transduced in Jurkat cells. Positively transduced cells were selected by puromycin (1 μg/mL).

Calcium Flux Analysis

Cells were loaded with 5 μM Indo-1 a.m. (ThermoFischer Scientific), washed, incubated with anti-CD4-APC and anti-CD8-FITC monoclonal antibodies (BD Biosciences, San Jose, CA), stimulated by anti-CD3 antibody (OKT3) crosslinked with F(ab′)2 rabbit anti-mouse immunoglobulin G (5 μg/mL; ThermoFischer Scientific), and then incubated with ionomycin (1 μM). Ca^{2+} flux kinetic was monitored using a FACSAria flow cytometer (BD Biosciences) and analyzed with FlowJo software (Tree Star, Ashland, OR). The ratio of Ca^{2+}-bound to Ca^{2+}-free Indo-1 fluorescence was plotted against time.

Statistical Analysis

Results were analyzed by 1-way analysis of variance using Prism (GraphPad Software, Inc., La Jolla, CA) and P values <0.05 were considered significant.

References

1. Charbit-Henrion F, et al. J Crohn's Colitis 2018;12(9):1104–1112.
2. **Parlato M, Charbit-Henrion F**, et al. Gastroenterology 2019;156:1206–1210.
3. Itan Y, et al. Nat Methods 2016;13:109–110.
4. Zhang P, et al. Bioinformatics 2018;34:4307–4309.
5. Duval R, et al. Sci Rep 2015;5:10750.
6. Iversen LF, et al. J Biol Chem 2002;277:19982–19990.
7. Goujon M, et al. Nucleic Acids Res 2010;38:W695–W699.
8. Schwede T. Nucleic Acids Res 2003;31:3381–3385.
9. Pettersen EF, et al. J Comput Chem 2004;25:1605–1612.

Author names in bold designate shared co-first authorship.

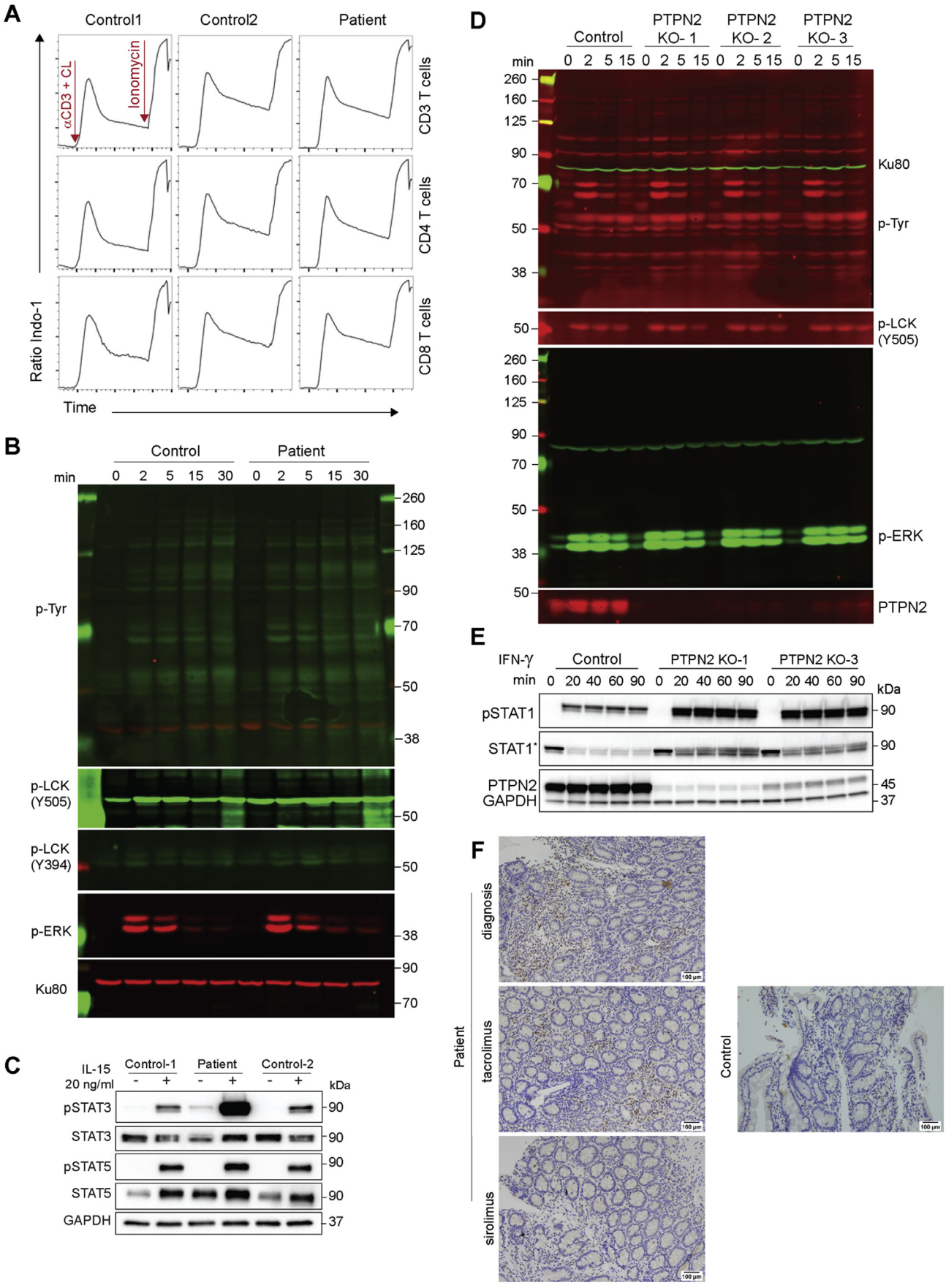

Supplementary Figure 1. Impact of PTPN2 depletion on JAK-STAT signaling and TCR activation in T-cell blasts from patient and in PTPN2-deficient Jurkat cells. *STAT1 antibody preferentially recognizes the nonphosphorylated form of STAT1.

Supplementary Table 1. Autosomal Recessive (AR) and De Novo Variants Identified by Whole Exome Sequencing

AR	Gene	Variant	Consequence	Sift	Mutation taster	Polyphen	CADD (MSC)	DB freq, %
	SRRM2	rs144257955	Thr2513Ala	Tolerated	Polymorphism	Benign	10 (3.13)	0.299
	LY75	rs116058499	Arg763Gln	Tolerated	Disease causing	Probably damaging	27 (3.13)	0.217
		rs113023766	Met1308Val	Tolerated	Polymorphism	Benign	23.9 (3.13)	0.137
	TDRD6	rs139660386	Lys1432Arg	Tolerated	Polymorphism	Benign	0 (3.13)	0.236
		rs144889394	Ala491Val	Deleterious	Disease causing	Probably damaging	24.3 (3.13)	0.020
	COL22A1	rs766709365	Asp156Glu	Deleterious	Disease causing	Probably damaging	14.7 (3.13)	0.005
		rs770249679	Arg407His	Deleterious	Disease causing	Probably damaging	23.7 (3.13)	0.001
	FOXD4L6	9_69200873_G_A	Pro247L	Tolerated	Not scored	Benign	8.3 (9.118)	0.265
		rs2989709	Pro416Arg	Tolerated	Not scored	Benign	0 (9.118)	0.210
	DOCK6	rs778570965	Asp1804Ala	Deleterious	Disease causing	Benign	25.1 (26.3)	0.001
		rs183060698	Val45Ile	Tolerated	Disease causing	Benign	19.8 (26.3)	0.180
de novo	**Gene**	**Variant**	**Consequence**	**Sift**	**Mutation taster**	**Polyphen**	**CADD**	
	NBPF1[a]	rs753338419	Asn497Ile	Deleterious	not scored	Probably damaging	22.7 (3.13)	0.011
	NES[a]	1_156640666_A_C	Val1105Gly	Deleterious	not scored	Benign	11.5 (3.13)	0.065
	HRCT1[a]	9_35906602_C_CCACCA	frameshift	not scored	not scored	not scored	0 (3.13)	not found
	DNASE1L[a]	16_2287508_G_C	Arg150Pro	Tolerated	not scored	Benign	0.1 (16.330)	0.099
	CSH1	rs1130686	Pro3Thr	Tolerated	Polymorphism	not scored	0	not found
	PTPN2	18_12817214_A_C	Cys216Gly	Deleterious	disease causing	Probably damaging	25.2 (3.13)	not found
	FUT3[a]	19_5844663_A_G	Leu63Pro	Tolerated	not scored	Benign	15.1 (3.13)	0.099
	ALPPL2[a]	rs139018608	Pro22Gln	Deleterious	Disease causing	Probably damaging	22.5 (3.13)	0.779
	USP36[a]	rs143011665	Arg1006Cys	Tolerated	Polymorphism	Benign	12 (3.13)	0.270
	SKA3[a]	13_21729290_T_TCAGTTTT CTTTGTTGCTGACATCT CGGATGTTCTGTCCATG TTTAAGGAACCTTTTA	ins/ splice acceptor donor	Not scored	Not scored	Not scored	0 (3.13)	0.043

CADD, Combined Annotation Dependent Depletion; DB, Public databases (dbSnp, 1000 genomes, Evs, Exac, and gnomAD); MSC, mutation significance cutoff.
[a]The variant was considered unlikely causative as in our inhouse database was found in at least 15 individuals.